PUBLISHED VERSION

Daniel J. Rankin, Lydéric Bocquet, and David M. Huang
Entrance effects in concentration-gradient-driven flow through an ultrathin porous membrane
Journal of Chemical Physics, 2019; 151(4):044705-1-044705-8

© 2019 Author(s). Published under license by AIP Publishing

This article may be downloaded for personal use only. Any other use requires prior permission of the author and AIP Publishing. This article appeared in ***Journal of Chemical Physics, 2019; 151(4):044705-1-044705-8*** and may be found at http://dx.doi.org/10.1063/1.5108700

PERMISSIONS

https://publishing.aip.org/resources/researchers/rights-and-permissions/sharing-content-online/

For institutional or funder-designated repositories (e.g., DOE Pages)

- You may deposit the accepted manuscript immediately after acceptance, using the credit line formatting below
- You may deposit the VOR 12 months after publication, with the credit line and a link to the VOR on AIP Publishing's site

Format for credit lines

- After publication please use: "This article may be downloaded for personal use only. Any other use requires prior permission of the author and AIP Publishing. This article appeared in (citation of published article) and may be found at (URL/link for published article abstract).
- Prior to publication please use: "The following article has been submitted to/accepted by [Name of Journal]. After it is published, it will be found at Link."
- For Creative Commons licensed material, please use: "Copyright (year) Author(s). This article is distributed under a Creative Commons Attribution (CC BY) License."

16 June 2021

http://hdl.handle.net/2440/130742

The Journal of Chemical Physics

Entrance effects in concentration-gradient-driven flow through an ultrathin porous membrane

Cite as: J. Chem. Phys. **151**, 044705 (2019); https://doi.org/10.1063/1.5108700
Submitted: 01 May 2019 . Accepted: 27 June 2019 . Published Online: 29 July 2019

Daniel J. Rankin, Lydéric Bocquet, and David M. Huang

COLLECTIONS

Paper published as part of the special topic on JCP Editors' Choice 2019

This paper was selected as an Editor's Pick

View Online Export Citation CrossMark

ARTICLES YOU MAY BE INTERESTED IN

Osmotic and diffusio-osmotic flow generation at high solute concentration. I. Mechanical approaches
The Journal of Chemical Physics **146**, 194701 (2017); https://doi.org/10.1063/1.4982221

Resonant osmosis across active switchable membranes
The Journal of Chemical Physics **152**, 054704 (2020); https://doi.org/10.1063/1.5138987

Osmotic and diffusio-osmotic flow generation at high solute concentration. II. Molecular dynamics simulations
The Journal of Chemical Physics **146**, 194702 (2017); https://doi.org/10.1063/1.4981794

Challenge us.
What are your needs for periodic signal detection?
Watch

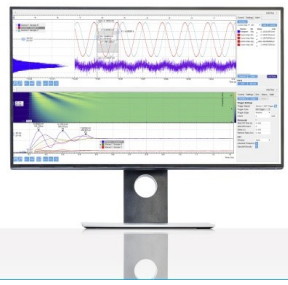

Zurich Instruments

AIP Publishing

© 2019 Author(s).

The Journal of Chemical Physics ARTICLE scitation.org/journal/jcp

Entrance effects in concentration-gradient-driven flow through an ultrathin porous membrane

Cite as: J. Chem. Phys. 151, 044705 (2019); doi: 10.1063/1.5108700
Submitted: 1 May 2019 • Accepted: 27 June 2019 •
Published Online: 29 July 2019

View Online Export Citation CrossMark

Daniel J. Rankin,[1] Lydéric Bocquet,[2] and David M. Huang[1,a)]

AFFILIATIONS

[1] Department of Chemistry, School of Physical Sciences, The University of Adelaide, Adelaide, Australia
[2] Laboratoire de Physique Statistique, CNRS UMR 8550, Ecole Normale Supérieure, PSL Research University, Paris, France

[a)] **Electronic mail:** david.huang@adelaide.edu.au

ABSTRACT

Transport of liquid mixtures through porous membranes is central to processes such as desalination, chemical separations, and energy harvesting, with ultrathin membranes made from novel 2D nanomaterials showing exceptional promise. Here, we derive, for the first time, general equations for the solution and solute fluxes through a circular pore in an ultrathin planar membrane induced by a solute concentration gradient. We show that the equations accurately capture the fluid fluxes measured in finite-element numerical simulations for weak solute–membrane interactions. We also derive scaling laws for these fluxes as a function of the pore size and the strength and range of solute–membrane interactions. These scaling relationships differ markedly from those for concentration-gradient-driven flow through a long cylindrical pore or for flow induced by a pressure gradient or an electric field through a pore in an ultrathin membrane. These results have broad implications for transport of liquid mixtures through membranes with thickness on the order of the characteristic pore size.

Published under license by AIP Publishing. https://doi.org/10.1063/1.5108700

I. INTRODUCTION

Fluid transport through pores and porous membranes plays a key role in many processes of fundamental and practical interest, including cellular homeostasis in biological systems,[1] chemical separations,[2] desalination,[3] and energy conversion.[4,5] Thus, a general theoretical understanding of the parameters that control these transport phenomena has broad implications for a variety of domains. Many theoretical models of fluid transport in porous membranes have considered flows only within the pores[6–9] and have neglected the effect of transport between the membrane pores and the fluid outside the membrane. These so-called entrance or access effects can dominate fluid transport processes when the membrane thickness approaches the characteristic pore size[10,11] or when the fluid–solid friction becomes small.[12,13] The most extreme examples of this situation are membranes of atomic thickness made from 2D materials such as graphene and its derivatives[14–19] or molybdenum sulfide.[20,21] Such 2D membranes are of great interest, as they have been shown to exhibit exceptional properties compared with conventional membranes for applications such as desalination[14] and electrical energy harvesting from salinity gradients.[20]

Fluid fluxes across a membrane can be induced by a variety of driving forces, including gradients of pressure, electrical potential, or solute concentration. Equations have previously been derived to quantify entrance effects on fluid flow driven by a pressure gradient[22,23] and on fluid flow[24] and ionic electrical currents[25,26] induced by an electric field acting on a electrolyte solution. However, to date, no theory has been developed to describe the entrance effects on fluid fluxes driven by concentration gradients and how they vary with relevant parameters.

Fluid fluxes driven by concentration gradients are of particular relevance in applications such as chemical separations,[2,16] desalination,[3,14,15,17] and salinity-gradient-driven energy harvesting.[4,5,13,20,27] This work focuses specifically on entrance effects on the concentration-gradient-driven process of diffusio-osmosis[28] in which the flow of a solute-containing solution is driven by an osmotic-pressure gradient that develops in the inhomogeneous interfacial fluid layer induced by interactions of the fluid with the solid surfaces. Diffusio-osmosis has been shown to play a key role in

Published under license by AIP Publishing

astonishing energy densities measured for salinity gradient energy harvesting in a nanotube membrane.[27] Thus, entrance effects on this phenomenon are of considerable interest.

Here we derive, for the first time, general equations to quantify the diffusio-osmotic solution flux and solute flux of a dilute solution through a circular aperture in a 2D membrane as a function of the aperture size and the strength and range of the interactions between the solute and membrane surface. We verify the accuracy of the equations by comparison with finite-element numerical simulations. We go on to compare the scaling behavior predicted for concentration-gradient-driven flow through a circular aperture with those for other membrane geometries and driving forces and discuss the implications of these results for real systems.

II. THEORY

A. Diffusio-osmotic flow

Consider the flow of a solution containing a single solute type through a circular aperture of radius a in an infinitesimally thin planar wall, as illustrated in Fig. 1. Assuming that the fluid flows can be described by continuum hydrodynamic equations for low-Reynolds-number steady-state flow of a dilute solution of an incompressible Newtonian fluid, the governing equations are[29]

$$-\nabla p - c\nabla U + \eta\nabla^2 \boldsymbol{u} = 0, \tag{1}$$

$$\nabla\cdot\boldsymbol{j} = \nabla\cdot\left(-D\nabla c - \mu c\nabla U + \boldsymbol{u}c\right) = 0, \tag{2}$$

$$\nabla\cdot\boldsymbol{u} = 0, \tag{3}$$

where $\boldsymbol{u}$, $\boldsymbol{j}$, p, and c are the solution velocity, solute current density, pressure, and solute concentration, respectively, η is the solution shear viscosity, and U is the solute–membrane interaction potential. D and μ are the solute diffusivity and mobility, respectively,

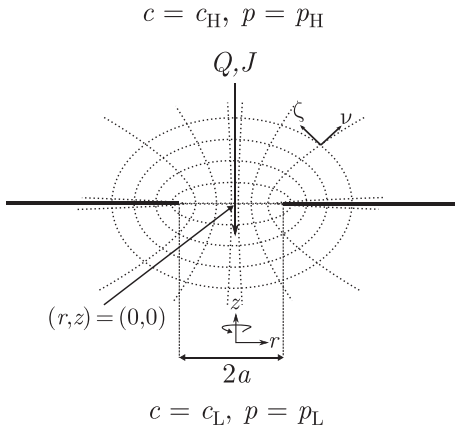

FIG. 1. Schematic of flow of a solution through a circular aperture of radius a in an infinitesimally thin planar wall. The origin in cylindrical (r, z) coordinates is at the center of the aperture, as indicated, and the axis of symmetry is the depicted z axis. The solute concentration c and solution pressure p far from the membrane are c_H and p_H, respectively, in the upper half-plane and c_L and p_L, respectively, in the lower half-plane. Q and J are the solution and solute fluxes, respectively. Contours of constant ζ and ν in oblate–spheroidal (ζ, ν) coordinates are also shown as dashed lines, with unit vectors shown at one point in space.

which we assume are related by the Einstein relation, $\mu = \frac{D}{k_B T}$,[30] where k_B is the Boltzmann constant and T is the temperature. U is the interaction potential per solute molecule and so $-c\nabla U$ is a body force per unit volume acting on the fluid due to the solute–membrane interactions. U is assumed to depend on the position in the fluid relative to the membrane surface. For a neutral solute, U typically depends on the distance from the surface[28,29] and has a range on the order of the solute molecular diameter. Further assuming that advection of the solute is negligible compared with diffusion (i.e., low Péclet number flow), Eq. (2) for the solute flux simplifies to

$$\nabla\cdot\boldsymbol{j} = \nabla\cdot\left(-D\nabla c - D\frac{c}{k_B T}\nabla U\right) = 0. \tag{4}$$

The solution velocity and solute flux are assumed to satisfy the usual no-slip and zero flux boundary conditions at the membrane surface, i.e., $\boldsymbol{u} = 0$ and $\hat{\boldsymbol{n}}\cdot\boldsymbol{j} = 0$, where $\hat{\boldsymbol{n}}$ is the unit vector normal to the membrane surface.

We note that a similar approach based on the widely used Poisson–Nernst–Planck–Stokes equations for electrolytes,[30] in which the electric potential energy plays an analogous role for the electrolyte that the interaction potential U does for a neutral solute, could be used to extend this study to concentration-gradient-driven electrolyte transport. However, such an extension is nontrivial, as the electric potential must be determined by solving an additional coupled differential equation (the Poisson equation) that depends on the solute (electrolyte) concentration, rather than being specified. Thus, we leave this extension to electrolytes to future work.

Consider the fluid flow induced by a concentration difference, $\Delta c = c_H - c_L$, between the two sides of the membrane, with the pressure far from the membrane the same on both sides of the membrane, i.e., $p_H = p_L = p_\infty$, as shown in Fig. 1.

Our derivation uses a combination of cylindrical (r, z, ϕ) and oblate spheroidal (ζ, ν, ϕ) coordinates, where $z = a\nu\zeta$, $r = a\sqrt{(1+\nu^2)(1-\zeta^2)}$, and ϕ is the angle about the z axis $(0 \le \nu < \infty, -1 \le \zeta \le 1$, and $0 \le \phi < 2\pi)$.[24,31] Writing the solute concentration in the presence of a concentration gradient as

$$c(\zeta,\nu) \equiv c_s(\zeta,\nu)e^{-U(\zeta,\nu)/k_B T}, \tag{5}$$

where $c_s(\zeta, \nu)$ is to be determined, and inserting this expression into Eq. (4) and the boundary condition for the solute current density $\boldsymbol{j}$ gives

$$\nabla^2 c_s - \nabla\left(\frac{U}{k_B T}\right)\cdot\nabla c_s = 0, \tag{6}$$

with the boundary condition $\hat{\boldsymbol{n}}\cdot\nabla c_s = 0$ at the membrane surface. If the solute–membrane interaction potential is small relative to the thermal energy ($U \ll k_B T$), Eq. (6) reduces to

$$\nabla^2 c_s = 0. \tag{7}$$

Solving this equation, subject to the boundary conditions on c_s at the membrane surface and far from the membrane ($c_s \to c_H = c_\infty + \frac{\Delta c}{2}$ and $c_L = c_\infty - \frac{\Delta c}{2}$ in the upper and lower half-planes, respectively, where $U \to 0$), gives[31]

Published under license by AIP Publishing

$$c_s = c_\infty + \frac{\Delta c}{\pi}\tan^{-1}\nu. \tag{8}$$

We have verified using finite-element numerical simulations (see Fig. S3 of the supplementary material) that Eq. (8) with Eq. (5) accurately describes the solute concentration even when U is several times k_BT. A possible reason why Eq. (8) appears to be accurate outside the regime for which it was derived is that the second term in Eq. (6) that was neglected to arrive at Eqs. (7) and (8) can be small even if the magnitude of the potential U is large: for example, for c_s given by Eq. (8), this term is zero for a potential that is a function only of ζ or in the pore mouth (at $\nu = z = 0$) for a potential that is a function only of the distance from the membrane, due to the orthogonality of ∇U and ∇c_s in these cases.

The fluid flow induced by the concentration gradient can be obtained from the reciprocal theorem for steady incompressible creeping flow,[32] which allows the fluid flow due to a body force $\boldsymbol{F}$ acting on the fluid to be related to the pressure-driven flow in the same pore geometry,[24] for which an analytical solution exists for the fluid velocity through a circular aperture.[22,32] As shown by Mao *et al.*[24] for the related problem of electroosmosis through a circular aperture,

$$Q = -\frac{1}{\Delta p}\iiint_V \mathrm{d}V\,\tilde{\boldsymbol{u}}\cdot\boldsymbol{F}, \tag{9}$$

where $\tilde{\boldsymbol{u}}$ is the fluid velocity induced by a pressure difference $\Delta p = p_H - p_L$ for $\Delta c = 0$ in the system geometry in Fig. 1 and the integral is over the volume V occupied by the fluid. For concentration-gradient-driven flow described by Eq. (1), $\boldsymbol{F} = -c\nabla U$. The pressure-driven flow velocity can be obtained from the stream function $\psi = -\frac{a^3}{6\pi\eta}\left(1-\zeta^3\right)\Delta p$ for the flow[32] using $\tilde{\boldsymbol{u}} = \frac{1}{r}\hat{\boldsymbol{\phi}}\times\nabla\psi$,[32] where $\hat{\boldsymbol{\phi}}$ is the unit vector in the ϕ direction, as

$$\tilde{\boldsymbol{u}} = -\frac{a\zeta^2\Delta p}{2\pi\eta\sqrt{(1+\nu^2)(\nu^2+\zeta^2)}}\,\hat{\boldsymbol{\nu}}. \tag{10}$$

Inserting this expression for $\tilde{\boldsymbol{u}}$ and $\boldsymbol{F} = -c\nabla U$ into Eq. (9) [with c given by Eqs. (5) and (8)] and making use of $\frac{\partial c_s}{\partial \nu} = \frac{\Delta c}{\pi}(1+\nu^2)^{-1}$ yields

$$Q = -\kappa_{DO}\Delta c, \tag{11}$$

with

$$\kappa_{DO} = -\frac{2k_BTa^3}{\pi\eta}\int_0^1 \mathrm{d}\zeta\,\zeta^2\int_0^\infty \mathrm{d}\nu\left(\frac{e^{-U/k_BT}-1}{1+\nu^2}\right). \tag{12}$$

Equation (12) is the main result of this work.

Furthermore, the solute flux density can be obtained, using Eqs. (4) and (5), as

$$\boldsymbol{j} = -De^{-U/k_BT}\nabla c_s. \tag{13}$$

The solute flux across the membrane is

$$J = \iint_S \mathrm{d}s\,\boldsymbol{j}\cdot\hat{\boldsymbol{n}}, \tag{14}$$

where the unit vector normal to the pore mouth is $\hat{\boldsymbol{n}} = \hat{\boldsymbol{\nu}} = \hat{\boldsymbol{z}}$ and the surface integral is over the pore aperture. Evaluating the solute flux at the pore mouth (at $\nu = z = 0$) using Eqs. (8) and (13) yields

$$J = -2Da\Delta c\int_0^1 \mathrm{d}\zeta\,e^{-U/k_BT} \tag{15}$$

$$= -2D\Delta c\int_0^a \frac{\mathrm{d}r\,re^{-U/k_BT}}{\sqrt{a^2-r^2}}. \tag{16}$$

B. Limiting cases and scaling behavior

The diffusio-osmotic mobility predicted in Eq. (12) depends crucially on the range of the interaction potential U, which we will call λ. However, the term $\exp(-U/k_BT) - 1$ in Eq. (12) is averaged spatially with a geometry-dependent weight, with a complicated dependence on the (oblate–spheroidal) coordinates ζ and ν. As a consequence, the mobility, and its scaling with the pore radius a and interaction range λ, may depend on specific details of the geometry dependence of the interaction. Therefore, we consider various limiting cases for the geometry of the potential and the consequences for the dependence of the scaling with the pore radius and interaction range.

1. Case of potential that depends only on the distance to the membrane surface and/or pore edge

In most circumstances, the potential U is expected to be a function of the distance d from the membrane surface. However, the integral in Eq. (12) for the mobility cannot be simplified due to the geometrical interplay between the various variables.

Let us assume for simplicity that the solute excess/depletion at the membrane surface can be represented by a step function as a function of the distance d from the surface, i.e.,

$$e^{-U(d)/k_BT} = \begin{cases}\alpha, & d \le \lambda\\ 1, & d > \lambda\end{cases}, \tag{17}$$

where α characterizes the solute excess close to the membrane surface ($\alpha > 1$ for solute adsorption and $\alpha < 1$ for solute depletion). While the mobility still cannot, in general, be evaluated analytically in this case, analytical solutions exist in certain limits. In particular, for a solute–wall interaction range much larger than the pore radius ($\lambda \gg a$), $e^{-U(d)/k_BT}$ can be approximated as a constant independent of the coordinates, and we find from Eq. (12) in this limit that

$$\kappa_{DO} \simeq -\frac{k_BT\Delta c}{3\eta}(\alpha-1)a^3. \tag{18}$$

On the other hand, if $\lambda \ll a$, the integral in Eq. (12) can be approximated as

$$\kappa_{DO} \simeq -\frac{k_BT}{\eta}\left(\frac{1}{4}+\frac{1}{\pi}\right)(\alpha-1)a\lambda^2. \tag{19}$$

Details of the derivation of this equation can be found in the supplementary material.

Published under license by AIP Publishing

A similar calculation can be performed for the case in which the interaction originates only from the pore edge, and U depends on the distance to the edge. As detailed in the supplementary material, the mobility in this case is

$$\kappa_{DO} \simeq -\frac{k_B T}{2\eta}(\alpha - 1) a \lambda^2. \tag{20}$$

Solute flux. Similarly, using Eq. (17) in Eq. (16) and noting that $d = a - r$ in the pore mouth at $z = 0$, the solute flux across the membrane for the step-function potential can be shown to be

$$J_{step} = -2D\Delta c\left[a + (\alpha - 1)\sqrt{\lambda(2a - \lambda)}\right] \tag{21}$$

for $\lambda \leq a$ and

$$J_{step} \simeq -2D\Delta c \alpha a \tag{22}$$

for $\lambda \gg a$.

2. Case of potential that depends only on ζ

In the case in which the potential U is a function of the ζ coordinate only (see Fig. 1), the diffusio-osmotic mobility in Eq. (12) simplifies to

$$\kappa_{DO} = -\frac{k_B T a^3 \Delta c}{\eta} \int_0^1 d\zeta\, \zeta^2 \left(e^{-U(\zeta)/k_B T} - 1\right). \tag{23}$$

Assuming that U only depends on ζ is a stringent condition in terms of symmetry, but interestingly such a result is expected for a circular aperture in a planar membrane at a fixed electrostatic potential (however, in the absence of screening).

To determine how Q scales with λ, particularly in the limit $\lambda \ll a$, we can use the relationship between ζ and the distances, d_1 and d_2, from a point with this ζ value to the two foci of the hyperbolae or ellipses of constant ζ or ν that are shown in Fig. 1. For an infinitesimally thin membrane, these foci are located at the pore edge (at $r = a$), and thus $1 - \zeta^2 = [(d_1 - d_2)/(2a)]^2$. So a potential $U(\zeta)$ that depends only on ζ depends only on the relative distance, $d_1 - d_2$. Furthermore, assuming that the potential has a distance range λ implies that $U(\zeta) = U[(a - |d_1 - d_2|/2)/\lambda]$. In addition, U is only nonzero when $a - |d_1 - d_2|/2 \sim \lambda \ll a$, so $a - |d_1 - d_2|/2 = a(1 - \sqrt{1 - \zeta^2}) \simeq a\zeta^2/2$ when the integrand in Eq. (23) is nonzero. Thus, in this limit, $U(\zeta) \sim U\left[a\zeta^2/(2\lambda)\right]$ and the integral in Eq. (23) becomes

$$\int_0^1 d\zeta\, \zeta^2 \left(e^{-U\left[a\zeta^2/(2\lambda)\right]/k_B T} - 1\right) \simeq (2\lambda/a)^{3/2} \int_0^\infty dx\, x^2 \left(e^{-U(x^2)/k_B T} - 1\right), \tag{24}$$

where $x \equiv [a/(2\lambda)]^{1/2}\zeta$. So the mobility in this case scales as $\kappa_{DO} \sim a^3(\lambda/a)^{3/2} \sim (a\lambda)^{3/2}$.

Equation (23) can also be rewritten in radial coordinates, by focusing on the pore mouth ($\nu = z = 0$), as

$$\kappa_{DO} = -\frac{k_B T}{\eta} \int_0^a dr\, r\sqrt{a^2 - r^2}\left(e^{-U/k_B T} - 1\right), \tag{25}$$

where r is the distance to the center of the pore in the membrane plane ($z = 0$). As an alternative approach to predicting the dependence of the mobility on λ, we again restrict ourselves, for simplicity, to a step-function interaction vs distance $d = a - r$ from the pore edge, i.e.,

$$e^{-U(r)/k_B T} = \begin{cases} \alpha, & a - r \leq \lambda \\ 1, & a - r > \lambda \end{cases}. \tag{26}$$

Inserting Eq. (26) into Eq. (25) gives the diffusio-osmotic mobility for the step-function potential as

$$\kappa_{DO} = -\frac{k_B T}{3\eta}(\alpha - 1)[\lambda(2a - \lambda)]^{3/2}. \tag{27}$$

For a small interaction range λ compared with the pore radius, the predicted scaling of the mobility is

$$\kappa_{DO} \simeq -\frac{k_B T}{3\eta}(\alpha - 1)(a\lambda)^{3/2}, \tag{28}$$

which is identical to the scaling predicted directly from Eq. (23).

3. Case of potential that depends only on ν

In the case in which the potential U is a function of the ν coordinate only (see Fig. 1), the diffusio-osmotic mobility in Eq. (12) simplifies to

$$\kappa_{DO} = -\frac{2k_B T a^3}{3\pi\eta} \int_0^\infty d\nu \left(\frac{e^{-U(\nu)/k_B T} - 1}{1 + \nu^2}\right). \tag{29}$$

Following similar reasoning to Sec. II B 2, in terms of the distances, d_1 and d_2, from a point with a given ν value to the foci of the ellipses or hyperbolae in Fig. 1, $1 + \nu^2 = [(d_1 + d_2)/(2a)]^2$. So a potential $U(\nu)$ that depends only on ν depends only on the average distance, $(d_1 + d_2)/2$. Therefore, assuming that the potential has a distance range λ entails $U(\nu) = U([(d_1 + d_2)/2 - a]/\lambda)$. For $\lambda \ll a$, $(d_1 + d_2)/2 - a = a(\sqrt{1 + \nu^2} - 1) \simeq a\nu^2/2$. Thus, in this limit, $U(\nu) \sim U[a\nu^2/(2\lambda)]$ and the integral in Eq. (29) becomes

$$\int_0^\infty d\nu \left(\frac{e^{-U\left[a\nu^2/(2\lambda)\right]/k_B T} - 1}{1 + \nu^2}\right) = (2\lambda/a)^{1/2} \int_0^\infty dx \left(\frac{e^{-U(x^2)/k_B T} - 1}{1 + (2\lambda/a)x^2}\right) \tag{30}$$

$$\simeq (2\lambda/a)^{1/2} \int_0^\infty dx \left(e^{-U(x^2)/k_B T} - 1\right), \tag{31}$$

where $x \equiv [a/(2\lambda)]^{1/2}\nu$. So the mobility in this case scales as $\kappa_{DO} \sim a^3(\lambda/a)^{1/2} \sim a^{5/2}\lambda^{1/2}$.

III. NUMERICAL RESULTS

To validate the theory, finite-element method (FEM) simulations of concentration-gradient-driven flow were carried out using Comsol Multiphysics (version 4.3a)[33] through pores with various radii and solute–membrane interactions. Here, we consider that the solute interacts with the membrane via a potential that depends on the (shortest) distance d to the membrane surface. Accordingly, the solute–membrane interaction potential was modeled using a hyperbolic tangent function,

Published under license by AIP Publishing

$$U(d) = \frac{\epsilon}{2}\left[1 - \tanh\left(\frac{d-\lambda}{\lambda}\right)\right], \tag{32}$$

defined by parameters ϵ and λ describing the strength and range of the potential. In all simulations, the average solute concentration c_∞ was $10^{-3}\sigma^{-3}$ and the solute diffusivity D was σ^2/τ, and unless otherwise stated, the aperture radius a was 10 σ and λ was σ, where σ is the unit of length (σ can be regarded as the diameter of a fluid molecule) and $\tau = \eta\sigma^3/(k_B T)$ is the unit of time. Details of the FEM simulations, which all correspond to low-Péclet number flow, are given in the supplementary material.

We have quantified the concentration-gradient-driven solution and solute fluxes measured in the numerical simulations and predicted by our theory in terms of the diffusio-osmotic mobility κ_{DO} defined by

$$\kappa_{DO} \equiv -\frac{Q}{\Delta c} \tag{33}$$

and the solute permeance P_s defined by

$$P_s \equiv -\frac{J}{\Delta c}. \tag{34}$$

The equations that we have derived for the solution and solute fluxes [Eqs. (12) and (15)] predict that the fluxes are linearly related to the concentration difference Δc and thus that the conductance and resistance defined in Eqs. (33) and (34) are independent of Δc. We have verified that this is indeed the case for the range of concentration differences studied in the numerical simulations ($\Delta c = 10^{-6}$ to 3×10^{-4} $\sigma^{-3} = 10^{-3}$ to 0.3 c_∞), as shown in Fig. S5 of the supplementary material.

Figure 2 shows the diffusio-osmotic mobility κ_{DO} from the simulations and theory of a circular aperture as a function of aperture radius a and solute–membrane interaction range λ for two different values of the solute–membrane interaction strength ϵ, $k_B T/10$ and $k_B T$, with all other parameters kept constant. The theory curves were calculated by numerically evaluating the integral in Eq. (12) with the solute–membrane potential U in Eq. (32). The sign of κ_{DO} has been defined so that positive and negative values correspond to fluid flow in the opposite and same direction, respectively, to the applied concentration gradient. Hence, for solute depletion at the membrane surface ($\epsilon > 0$), the flow is toward higher solute concentration ($\kappa_{DO} < 0$), whereas for solute adsorption, the flow is toward lower concentration ($\kappa_{DO} > 0$).[34]

Figure 2 shows good quantitative agreement between the theory and simulations for the variation of κ_{DO} with all relevant parameters for $\epsilon \lesssim k_B T$. Since the theory assumes a weak potential in deriving Eq. (8) for the solute concentration, we indeed find deviations between the prediction and the simulations as the magnitude of the solute–membrane potential increases. Nevertheless, the agreement is reasonable well beyond the regime of validity of this approximation. Note that for the values of ϵ in Fig. 2, $\alpha - 1 \approx e^{-\epsilon/k_B T} - 1 \approx -\epsilon/k_B T$, and so from Eq. (18) or (19), κ_{DO} is approximately proportional to ϵ, but this scaling is not expected, in general, and already starts to break down for $\epsilon = k_B T$.

Figure 2 also compares the simulation results with the approximate scaling with the pore radius a and solute–membrane interaction range λ predicted by the theory. For $a \ll \lambda$, Eq. (18) predicts that

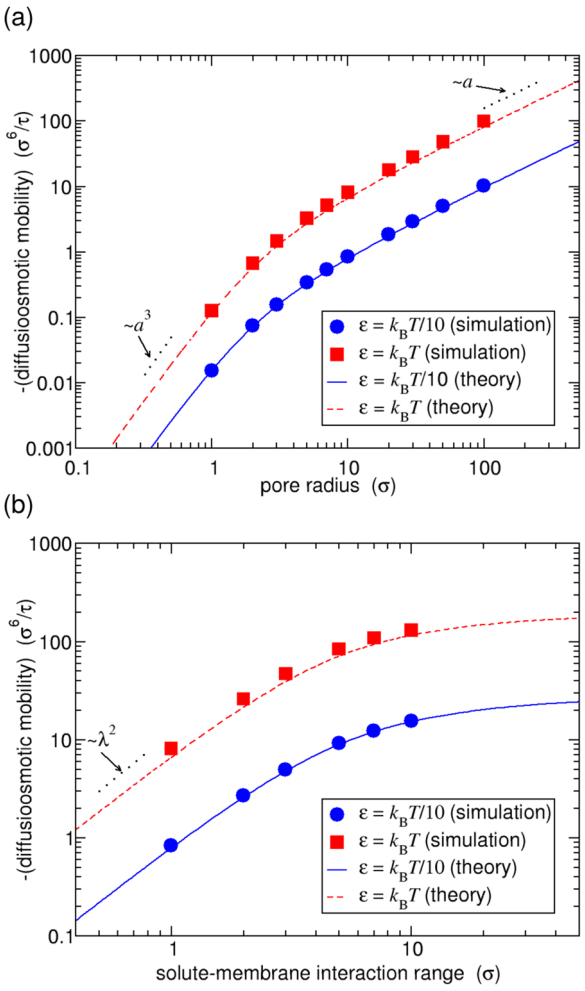

FIG. 2. Diffusio-osmotic mobility κ_{DO} vs (a) pore radius a (with $\lambda = \sigma$) and (b) solute–membrane interaction range λ (with $a = 10\sigma$) for solute–membrane interaction strength $\epsilon = k_B T/10$ or $k_B T$ from FEM simulations (points) and theory (solid and dashed lines). The dotted lines show scaling with various powers of a and λ.

κ_{DO} is proportional to a^3 and independent of λ, which is evident in the scaling for small a in Fig. 2(a) and in the saturation at large λ in Fig. 2(b). On the other hand, for $a \gg \lambda$, Eq. (19) predicts scaling of κ_{DO} with $a\lambda^2$, which is seen to hold in the large-a regime in Fig. 2(a) and in the small-λ regime in Fig. 2(b).

Figure 3 shows the analogous comparison between the FEM simulations and theory for the solute permeance P_s. The theory curves were calculated by numerically evaluating the integral in Eq. (16) with the solute–membrane potential U in Eq. (32). As for the diffusio-osmotic conductance, the theory accurately captures the simulated solute permeance for $\epsilon \lesssim k_B T$, with deviations between the theory and simulations becoming evident for magnitudes of the solute–membrane potential greater than $k_B T$. For the parameters used in Fig. 3(a), the first term in Eq. (21) dominates and so the permeance P_s shows the expected linear scaling with the pore radius a. For $\lambda \ll a$, Eq. (21) predicts that P_s varies

Published under license by AIP Publishing

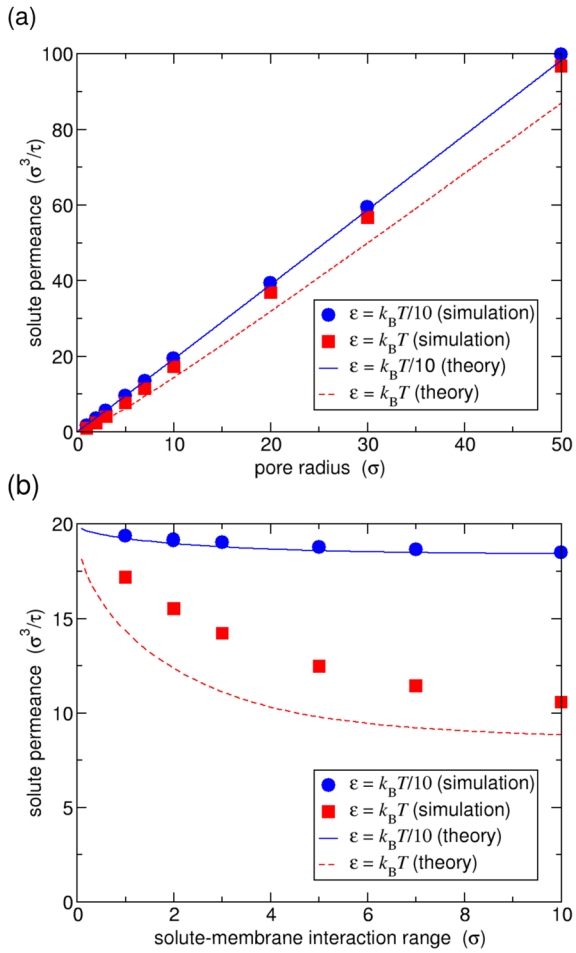

FIG. 3. Solute permeance P_s vs (a) pore radius a (with $\lambda = \sigma$) and (b) solute–membrane interaction range λ (with $a = 10\sigma$) for solute–membrane interaction strength $\epsilon = k_BT/10$ or k_BT from FEM simulations (points) and theory (lines).

from its value at $\lambda = 0$ with a scaling as $\sqrt{\lambda}$, which is evident in Fig. 3(b).

IV. DISCUSSION

An interesting outcome of the previous results is that the diffusio-osmotic mobility $\kappa_{DO} = -Q/\Delta c$ across a circular aperture in an ultrathin membrane is strongly dependent on the details of the interaction of the solute with the membrane. We have shown, in particular, that the mobility scales with the pore radius a and interaction range λ as $a^{3-\gamma}\lambda^{\gamma}$, with an exponent γ that depends on the underlying symmetries of the potential: when $\lambda \ll a$, for a potential that depends only on the ζ coordinate (in the oblate-spheroidal system, see Fig. 1), an exponent $\gamma = 3/2$ is predicted, for a potential that depends only on the ν coordinate, an exponent $\gamma = 1/2$ is predicted, whereas for a potential depending on the distance to the membrane, a value $\gamma = 2$ is found.

It is also interesting to compare the results for the circular aperture with those obtained in long cylindrical pores (e.g., as a model for nanotubes). As derived in detail in the supplementary material, the diffusio-osmotic mobility of a long cylindrical pore of length L is proportional to $(a\lambda)^2/L$ for $\lambda \ll a$. When compared to the case leading to an exponent $\gamma = 2$, the scaling of κ_{DO} with pore size and interaction range λ is therefore recovered by replacing the length of the nanopore L with the pore size a, which is indeed expected for entrance effects. However, as shown with the case leading to an exponent $\gamma = 3/2$ or $1/2$ for the diffusio-osmotic mobility, this situation is not universal. The different scaling relationships derived for κ_{DO} for a circular aperture and a long cylindrical pore are summarized in Table I.

These result are relevant for transport through finite-length pores, for which the total resistance to flow can often be accurately given by the sum of the resistance due to the pore interior and that due to the pore ends, which can be approximated by that of a circular aperture.[13,23,26]

The predicted scaling behavior of the diffusio-osmotic mobility and solute permeance of a circular aperture for concentration-gradient-driven flow differs markedly from the scaling behavior derived previously for other types of flows in the same system geometry. For example, the hydraulic conductance (solution flux per unit pressure difference) in pressure-driven fluid flow through a circular aperture has been shown[22,23,32] to be proportional to a^3 in contrast to the proportionality with $a^{3-\gamma}$ where $\gamma > 0$ for the diffusio-osmotic mobility in concentration-gradient-driven flow in the limit $\lambda \ll a$.

On the other hand, for $\lambda \gg a$, the diffusio-osmotic mobility shows the same a^3 scaling as the hydraulic conductance. The equivalent scaling of the hydraulic conductance and diffusio-osmotic mobility in this limit is because concentration-driven-flow in which the solute–membrane interaction range is larger than the aperture radius is equivalent to osmotic transport through a semipermeable membrane, with the osmotic pressure gradient due to the concentration gradient playing an equivalent role to the pressure gradient in pressure-driven flow.[35] Likewise, the scaling behavior predicted here for the diffusio-osmotic mobility differs from the electro-osmotic conductance for electric-field-driven fluid flow of an electrolyte, which has been shown to be proportional to a^3/λ_D for $a \ll \lambda_D$,[24] where λ_D is the Debye length characterizing the electric double layer width, equivalent to λ here; in the same

TABLE I. Scaling of the diffusio-osmotic mobility κ_{DO} with pore radius a and solute–membrane interaction range λ for a circular aperture in a 2D membrane, as well as with pore length L for a long cylindrical pore, for different functional forms of the solute–membrane potential U in the limits $\lambda \ll a$ and $\lambda \gg a$.

System	Limit	Potential	Scaling
Circular aperture	$\lambda \ll a$	$U(d)$	$a\lambda^2$
	$\lambda \ll a$	$U(\zeta)$	$a^{3/2}\lambda^{3/2}$
	$\lambda \ll a$	$U(\nu)$	$a^{5/2}\lambda^{1/2}$
	$\lambda \gg a$	Any	a^3
Cylinder	$\lambda \ll a$	$U(d)$	$a^2\lambda^2/L$
	$\lambda \gg a$	Any	a^4/L

Published under license by AIP Publishing

limit, scaling of the diffusio-osmotic mobility with a^3 is predicted here.

The electrical conductance across a circular aperture in electric-field-driven transport of an electrolyte has been shown to be proportional to a for an uncharged membrane,[25] with the addition of surface charge to the membrane only changing the length scale in the scaling relationship to an effective radius a_{eff} that is the sum of the aperture radius and the Dukhin length characterizing the ratio of the surface electrical conductivity to the bulk electrical conductivity,[26] without changing the scaling exponent. This scaling differs from that derived for the solute permeance for $\lambda \leq a$, for which the equivalent effective radius is $a_{\mathrm{eff}} = \left[a + (\alpha - 1)\sqrt{\lambda(2a - \lambda)}\right]$ in which the second term in the sum depends on both the solute–membrane interaction range λ and pore radius a.

We can consider the implications of our theory for realistic systems, in particular, for diffusio-osmotic transport of electrolyte solutions. Extending the theory to electrolytes is desirable for applications, such as salinity-gradient-driven energy conversion[4,20,27] and desalination,[3,14,15,17] but it is technically difficult, so we leave this derivation for future work. However, as a rule of thumb, one may expect that this would amount to replacing the solute–membrane interaction range λ by the salt-concentration-dependent Debye length $\lambda_{\mathrm{D}} \propto c_{\mathrm{salt}}^{-1/2}$. A counterintuitive outcome of the nonuniversal dependence of the diffusio-osmotic mobility as a function of the interaction range λ is a possible impact on the dependence of the mobility on the salt concentration. In a long pore under a salinity difference Δc_{salt}, the solvent flux is predicted to behave as $Q = K_{\mathrm{DO}} \Delta \log c_{\mathrm{salt}}$, with the mobility $K_{\mathrm{DO}} \propto c_{\mathrm{salt}}^{0} \pi a^2 / L$ for a long pore of length L,[27] i.e., no dependence of κ_{DO} on the salt concentration. This is due to the dependence of the diffusio-osmotic mobility $\kappa_{\mathrm{DO}} \sim \lambda_D^2 \sim c_{\mathrm{salt}}^{-1}$ so that $Q \sim \Delta \log c_{\mathrm{salt}}$. Now, for a circular aperture, we have shown that the dependence of the diffusio-osmotic mobility κ_{DO} on the interaction range scales as $\kappa_{\mathrm{DO}} \sim \lambda^{\gamma}$ with a nonuniversal exponent γ. Thus, the case of $\gamma = 2$ (occurring for potentials that depend on the distance to the membrane) will lead to $K_{\mathrm{DO}} \propto c_{\mathrm{salt}}^{0}$ as for the long-pore case, but cases with $\gamma \neq 2$ (as highlighted above in two cases) will lead to $K_{\mathrm{DO}} \propto c_{\mathrm{salt}}^{1-\gamma/2}$, exhibiting therefore a curious dependence on c_{salt}.

V. CONCLUSIONS

In summary, we have derived general equations and scaling relationships as a function of the pore radius and solute–membrane interaction strength and range for the solution and solute fluxes induced by a solute concentration gradient through a circular aperture in an ultrathin planar membrane. We have shown, by comparing with finite-element numerical simulations, that the equations accurately quantify the fluid fluxes when the solute–membrane interaction strength is small compared with the thermal energy $k_{\mathrm{B}}T$. In the limit of a solute–membrane interaction range much smaller than the pore radius, the theory predicts a nonuniversal dependence of the fluid fluxes on the pore radius and interaction range. These results have significant implications for applications involving concentration-gradient-driven flow in membranes in which the thickness is on the order of the pore size, such as those made from 2D nanomaterials, notably in the context of blue energy harvesting.

SUPPLEMENTARY MATERIAL

See supplementary material for derivations of scaling laws for diffusio-osmosis through a circular aperture in an ultrathin planar membrane, the theory of concentration-gradient-driven flow in a long cylindrical pore, and further details and supplementary results of finite-element numerical simulations.

ACKNOWLEDGMENTS

D.J.R. acknowledges the support of an Australian Government Research Training Program Scholarship and a University of Adelaide Faculty of Sciences Divisional Scholarship. L.B. acknowledges funding from the EU H2020 Framework Programme/ERC Advanced Grant Agreement No. 785911—Shadoks and ANR project Neptune.

REFERENCES

[1] H. X. Sui, B. G. Han, J. K. Lee, P. Walian, and B. K. Jap, "Structural basis of water-specific transport through the AQP1 water channel," Nature **414**, 872–878 (2001).
[2] J. R. Werber, C. O. Osuji, and M. Elimelech, "Materials for next-generation desalination and water purification membranes," Nat. Rev. Mater. **1**, 16018 (2016).
[3] M. Elimelech and W. A. Phillip, "The future of seawater desalination: Energy, technology, and the environment," Science **333**, 712–717 (2011).
[4] B. E. Logan and M. Elimelech, "Membrane-based processes for sustainable power generation using water," Nature **488**, 313–319 (2012).
[5] A. Siria, M.-L. Bocquet, and L. Bocquet, "New avenues for the large-scale harvesting of blue energy," Nat. Rev. Chem. **1**, 0091 (2017).
[6] J. C. Fair and J. F. Osterle, "Reverse electrodialysis in charged capillary membranes," J. Chem. Phys. **54**, 3307–3316 (1971).
[7] D. J. Bonthuis, K. F. Rinne, K. Falk, C. N. Kaplan, D. Horinek, A. N. Berker, L. Bocquet, and R. R. Netz, "Theory and simulations of water flow through carbon nanotubes: Prospects and pitfalls," J. Phys.: Condens. Matter **23**, 184110 (2011).
[8] S. Balme, F. Picaud, M. Manghi, J. Palmeri, M. Bechelany, S. Cabello-Aguilar, A. Abou-Chaaya, P. Miele, E. Balanzat, and J. M. Janot, "Ionic transport through sub-10 nm diameter hydrophobic high-aspect ratio nanopores: Experiment, theory and simulation," Sci. Rep. **5**, 10135 (2015).
[9] P. B. Peters, R. van Roij, M. Z. Bazant, and P. M. Biesheuvel, "Analysis of electrolyte transport through charged nanopores," Phys. Rev. E **93**, 053108 (2016).
[10] J. D. Sherwood, M. Mao, and S. Ghosal, "Electroosmosis in a finite cylindrical pore: Simple models of end effects," Langmuir **30**, 9261–9272 (2014).
[11] D. V. Melnikov, Z. K. Hulings, and M. E. Gracheva, "Electro-osmotic flow through nanopores in thin and ultrathin membranes," Phys. Rev. E **95**, 063105 (2017).
[12] T. Sisan and S. Lichter, "The end of nanochannels," Microfluid. Nanofluid. **11**, 787–791 (2011).
[13] D. J. Rankin and D. M. Huang, "The effect of hydrodynamic slip on membrane-based salinity-gradient-driven energy harvesting," Langmuir **32**, 3420–3432 (2016).
[14] S. P. Surwade, S. N. Smirnov, I. V. Vlassiouk, R. R. Unocic, G. M. Veith, S. Dai, and S. M. Mahurin, "Water desalination using nanoporous single-layer graphene," Nat. Nanotechnol. **10**, 459–464 (2015).
[15] D. Cohen-Tanugi, L.-C. Lin, and J. C. Grossman, "Multilayer nanoporous graphene membranes for water desalination," Nano Lett. **16**, 1027–1033 (2016).
[16] A. Morelos-Gomez, R. Cruz-Silva, H. Muramatsu, J. Ortiz-Medina, T. Araki, T. Fukuyo, S. Tejima, K. Takeuchi, T. Hayashi, M. Terrones, and M. Endo, "Effective NaCl and dye rejection of hybrid graphene oxide/graphene layered membranes," Nat. Nanotechnol. **12**, 1083–1088 (2017).

Published under license by AIP Publishing

[17]X. Li, W. Xu, M. Tang, L. Zhou, B. Zhu, S. Zhu, and J. Zhu, "Graphene oxide-based efficient and scalable solar desalination under one sun with a confined 2D water path," Proc. Natl. Acad. Sci. U. S. A. **113**, 13953–13958 (2016).
[18]M. I. Walker, K. Ubych, V. Saraswat, E. A. Chalklen, P. Braeuninger-Weimer, S. Caneva, R. S. Weatherup, S. Hofmann, and U. F. Keyser, "Extrinsic cation selectivity of 2D membranes," ACS Nano **11**, 1340–1346 (2017).
[19]L. Wang, M. S. H. Boutilier, P. R. Kidambi, D. Jang, N. G. Hadjiconstantinou, and R. Karnik, "Fundamental transport mechanisms, fabrication and potential applications of nanoporous atomically thin membranes," Nat. Nanotechnol. **12**, 509 (2017).
[20]J. Feng, M. Graf, K. Liu, D. Ovchinnikov, D. Dumcenco, M. Heiranian, V. Nandigana, N. R. Aluru, A. Kis, and A. Radenovic, "Single-layer MoS_2 nanopores as nanopower generators," Nature **536**, 197–200 (2016).
[21]W. Li, Y. Yang, J. K. Weber, G. Zhang, and R. Zhou, "Tunable, strain-controlled nanoporous MoS_2 filter for water desalination," ACS Nano **10**, 1829–1835 (2016).
[22]R. A. Sampson, "On Stokes's current function," Philos. Trans. R. Soc., A **182**, 449–518 (1891).
[23]H. L. Weissberg, "End correction for slow viscous flow through long tubes," Phys. Fluids **5**, 1033–1036 (1962).
[24]M. Mao, J. Sherwood, and S. Ghosal, "Electro-osmotic flow through a nanopore," J. Fluid Mech. **749**, 167–183 (2014).
[25]J. E. Hall, "Access resistance of a small circular pore," J. Gen. Physiol. **66**, 531–532 (1975).
[26]C. Lee, L. Joly, A. Siria, A.-L. Biance, R. Fulcrand, and L. Bocquet, "Large apparent electric size of solid-state nanopores due to spatially extended surface conduction," Nano Lett. **12**, 4037–4044 (2012).
[27]A. Siria, P. Poncharal, A.-L. Biance, R. Fulcrand, X. Blase, S. T. Purcell, and L. Bocquet, "Giant osmotic energy conversion measured in a single transmembrane boron nitride nanotube," Nature **494**, 455–458 (2013).
[28]J. L. Anderson, "Colloid transport by interfacial forces," Annu. Rev. Fluid Mech. **21**, 61–99 (1989).
[29]J. L. Anderson, M. E. Lowell, and D. C. Prieve, "Motion of a particle generated by chemical gradients Part 1. Non-electrolytes," J. Fluid Mech. **117**, 107–121 (1982).
[30]R. F. Probstein, *Physicochemical Hydrodynamics: An Introduction*, 2nd ed. (Wiley-Interscience, Hoboken, 1994).
[31]P. M. Morse and H. Feshbach, *Methods of Theoretical Physics* (McGraw-Hill Book Company, 1953), Vol. 2, p. 1292.
[32]J. Happel and H. Brenner, *Low Reynolds Number Hydrodynamics* (Martinus Nihjoff Publishers, 1983).
[33]See https://www.comsol.com for Comsol 4.3a.
[34]D. M. Huang, C. Cottin-Bizonne, C. Ybert, and L. Bocquet, "Massive amplification of surface-induced transport at superhydrophobic surfaces," Phys. Rev. Lett. **101**, 064503 (2008).
[35]S. Marbach, H. Yoshida, and L. Bocquet, "Osmotic and diffusio-osmotic flow generation at high solute concentration. I. Mechanical approaches," J. Chem. Phys. **146**, 194701 (2017).

Published under license by AIP Publishing